Nanoscale

PAPER

Check for updates

Cloudberry-derived nanovesicles as stable oral drug delivery systems: gastrointestinal stability and age-related biodistribution in mice

Keerthanaa Balasubramanian Shanthi,†[a] Feby Wijaya Pratiwi, [iD] *†[a,b]
Florence Naillat,‡[a] Ramila Mammadova, [iD] ‡[a] Marjaana Sarpola,[a] Si-Han Wu, [iD] *[c]
Marko Suokas,[d] Soile Jokipii-Lukkari, [iD] [d] Susanna Kaisto,[a] Anatoliy Samoylenko, [iD] [a]
Henrikki Liimatainen, [iD] [e] Caglar Elbuken[b,f] and Seppo Juhani Vainio [iD] *[a,b]

Plant-derived nanovesicles (PDNVs) have emerged as promising candidates for oral drug delivery due to their natural biocompatibility and ability to transport bioactive molecules. However, their stability within the gastrointestinal (GI) tract and efficacy in aging populations remain largely unexplored. In this study, we isolated nanovesicles from cloudberries (*Rubus chamaemorus*), which are rich in bioactive polyphenols, to evaluate their potential as stable oral drug delivery vehicles. We characterized the physical properties and RNA content of these cloudberry-derived nanovesicles (CNVs) and investigated their stability under simulated GI conditions *in vitro*. The CNVs maintained their structural integrity and functional properties after exposure to harsh digestive conditions, demonstrating resilience against digestive enzymes and pH variations. Using Caco-2 cell monolayers, we confirmed efficient cellular uptake and trans-epithelial transport of CNVs without inducing cytotoxic effects. Furthermore, we assessed the biodistribution and immune responses to CNVs in both young and elderly mice. *In vivo* imaging revealed favorable biodistribution patterns, prolonged retention in the GI tract, effective intestinal absorption, transfer to the bloodstream, and low immunogenicity in both age groups. Notably, aging influenced the biodistribution of CNVs, with elderly mice exhibiting delayed gastric emptying and prolonged GI retention, likely due to age-related physiological changes. These findings suggest that CNVs are promising, stable, and biocompatible oral drug delivery systems suitable for both young and elderly populations, highlighting their potential for therapeutic applications, especially in age-related conditions.

1. Introduction

In 1836, the German philosopher Ludwig Feuerbach famously claimed, "A man is what he eats".[1] This statement has gained new relevance as recent research suggests that food provides more than just nutrients; it can also deliver information from ingested plants that affect mammalian genes.[2] This information is transmitted by extracellular nanovesicles (NVs), which transport bioactive molecules like proteins, lipids, mRNAs, and miRNAs to consuming organisms. For example, plant-derived nanovesicles (PDNVs) from grapes, grapefruit, ginger, and carrots have shown anti-inflammatory properties and can modulate vascular cell responses.[3,4] Ginger PDNVs inhibit inflammasome activation, citrus-lemon and orange PDNVs possess antioxidant and antitumor properties,[3,4] Yam-PDNV stimulate osteoblast formation,[5] and apple-derived NVs can impact intestinal transporters.[6,7] Moreover, PDNVs can be successfully isolated in large quantities and at a low cost.[8,9] These discoveries highlight the therapeutic potential of PDNVs.

Despite extensive research on extracellular vesicles (EVs) and PDNVs, as well as their therapeutic applications, there is limited knowledge of their influence on aged cohorts and *in vivo* trafficking in elderly organisms. Aging impacts

[a]*Laboratory of Developmental Biology, Disease Networks Research Unit, Faculty of Biochemistry and Molecular Medicine, University of Oulu, FI-90014 Oulu, Finland. E-mail: feby.pratiwi@oulu.fi, seppo.vainio@oulu.fi*
[b]*Kvantum Institute, University of Oulu, 90014 Oulu, Finland*
[c]*Graduate Institute of Nanomedicine and Medical Engineering, Taipei Medical University, Taipei 11031, Taiwan. E-mail: smilehanwu@tmu.edu.tw*
[d]*Ecology and Genetics Department, University of Oulu, FI-90014 Oulu, Finland*
[e]*Fiber and Particle Engineering Research Unit, University of Oulu, FI-90014 Oulu, Finland*
[f]*Micro-/Nanofluidics and Biosensor Research Group, University of Oulu, FI-90014 Oulu, Finland*
† Equal first coauthor.
‡ Equal second coauthor.

absorption, distribution, metabolism, and excretion processes, often impairing drug efficacy and increasing toxicity risks—factors likely relevant for PDNVs as well.[10] Age-related changes, such as reduced gastric acid secretion, slower gastric emptying, decreased splanchnic blood flow, altered microbiota, and diminished solute transporter function, can delay drug dissolution and lower absorption.[11,12] Shifts in body composition (*e.g.*, increased body fat, decreased total body water) affect drug distribution, with lipophilic drugs exhibiting prolonged half-lives and hydrophilic drugs reaching higher plasma levels. Declines in liver function (*e.g.*, cytochrome P450 activity) and renal function (*e.g.*, glomerular filtration rate) further reduce drug clearance.[13] Given these age-related changes, careful dose adjustments and monitoring are essential to manage efficacy and reduce toxicity. Therefore, understanding PDNV behavior in elderly organisms is crucial for safe and effective application in this demographic.[10]

From a drug delivery perspective, the *in vivo* distribution and transport of PDNVs are critical, as they determine whether their bioactive component reaches the intended target tissues while minimizing off-target accumulation. PDNVs originate from edible sources and are naturally ingested as part of the human diet, making oral administration a biologically relevant and physiologically compatible route. This approach also reduces the risk of adverse immune reactions and avoids the invasiveness of intravenous (IV) or intraperitoneal (IP) injections.[14] As such, oral delivery is better suited for long-term or preventive use, particularly in chronic conditions and in vulnerable populations such as the elderly, who are also more prone to gastrointestinal (GI)-related diseases.[15] However, the specific properties of the digestive tract—including digestive enzymes, cellular and mucus barriers, and varying pH levels—pose challenges to drug absorption and limit bioavailability. PDNVs, with their compelling physicochemical properties like size distribution, charge, and elasticity, offer a promising solution. Moreover, unstable drug molecules, genes, or proteins can be loaded within their lumen, enhancing therapeutic effects. Therefore, PDNVs represent a promising platform for next-generation oral biotherapeutics, especially for targeting gastrointestinal conditions such as colitis, microbiota imbalance, and GI cancers.[16] Despite their potential, our understanding of the interactions between orally administered PDNVs and the GI environment remains limited, necessitating further exploration.

To address these challenges, we thoroughly investigated the behavior and interactions of PDNVs in gut environments, examining their presence both *in vitro* and *in vivo*. A promising source of PDNVs is the cloudberry (*Rubus chamaemorus*), a perennial herb thriving in boreal regions, particularly in bogs. These amber-colored berries, known for their juiciness and fragrance, are rich in nutrients such as vitamin C, ellagic acid, citric acid, malic acid, α-tocopherol, anthocyanins, and provitamin A carotenoid β-carotene. They also contain polyphenols, specifically ellagitannins, which offer potential health benefits such as potent antimicrobial, anti-adhesion, anti-inflammatory, antifungal, and anti-carcinogenic properties.[17] Thus, we used cloudberry-derived nanovesicles (CNVs) as a PDNV model in this study.

The main objective of this study is to assess the safety, biodistribution, and structural stability of CNVs following oral administration in both young and aged healthy mouse models. We envision CNVs serving a dual purpose: (1) as therapeutic agents through their native bioactive composition—including metabolites, lipids, proteins, glycans, and miRNAs—and (2) as nanocarriers for the targeted delivery of exogenous therapeutic payloads. We first evaluated the physicochemical stability and functional properties of CNVs under simulated gastrointestinal conditions using a validated *in vitro* digestion model. Investigated the effects of digestive processes on CNV stability and functional changes using a validated *in vitro* digestion model that simulates GI conditions. This was followed by using Caco-2 cells, a widely recognized human intestinal epithelial cell model, to demonstrate the uptake and *trans*-epithelial transport of CNVs across the cell monolayer. Additionally, we assessed their toxicity and antioxidant properties after the digestion process. Recognizing the importance of understanding how aging influences PDNV efficacy, we extended our investigation to include an age-related *in vivo* experiment. We administered CNVs to both elderly and young mice to assess how age affects the biodistribution of PDNVs and the immune response they cause. By comparing the biodistribution profiles and immune responses between the two age groups, we aimed to gain insight into the potential therapeutic applications of CNVs in elderly populations, where the need for effective, less invasive, and safe treatments is critical.

2. Materials and methods

2.1 Isolation of cloudberry-derived nanovesicles

To produce cloudberry juice containing cloudberry nanovesicles (CNVs), 250 g of cloudberries (Lapland, Finland) were mixed with an extraction buffer in a 1 : 1 weight-to-volume ratio containing protease inhibitors. The mixture was ground, squeezed, and filtered using a cheesecloth to remove any flesh, skin, and seeds. The extraction buffer consisted of 100 mM phosphate and 10 mM ethylenediaminetetraacetic acid (EDTA) (Merck, Darmstadt, Germany) at pH 8. A protease inhibitor cocktail was added per 100 mL of buffer, comprising 0.05 mL of 1 mg mL^{-1} leupeptin (Roche, Germany), 0.25 mL of 100 mM phenylmethylsulfonyl fluoride (PMSF) (Merck, Germany), and 0.16 mL of 1 M sodium azide (Merck, Germany).[18] The sample underwent sequential centrifugation at 2000g and 4000g for 30 minutes at 20 °C. The supernatant after the 4000g step was centrifuged at 15 000g in a 50 mL conical Eppendorf tube for 30 minutes at 20 °C, and the pellet containing microvesicles (MVs) was collected. The supernatant from the 15 000g step was subjected to ultracentrifugation at 100 000g for 2 hours at 4 °C using a SW28Ti rotor in a Beckman Optima L-100K ultracentrifuge. The pellet containing CNVs was collected and resuspended in a small volume of extraction buffer. The protein concentration was determined

using the Qubit Protein Assay Kit (Thermo Fisher Scientific, USA) according to the manufacturer's instructions.

2.2 RNA isolation from CNVs

CNV RNAs were isolated using QIAzol® Lysis Reagent (Qiagen, Hilden, Germany; cat. no. 79306), followed by RNA extraction using RNeasy® UCP MinElute® columns (Qiagen, Hilden, Germany; cat. no. 74204). Specifically, 115 µL of CNVs were mixed with 585 µL of QIAzol® Lysis Reagent. The mixture was vortexed briefly and incubated at room temperature for 5 minutes. Then, 80 µL of chloroform was added and mixed by inverting the tube 15 times. The mixture was centrifuged at 12 000g at 4 °C for 15 minutes. The aqueous top layer was carefully removed without disturbing the interphase. Two volumes of absolute ethanol were added to the aqueous phase, and the solution was gently mixed. The solution was loaded onto RNeasy® UCP MinElute® columns in 700 µL increments and centrifuged at 12 000 rpm for 15 seconds. After discarding the flow-through, the column was washed with 700 µL of manufacturer-supplied RWT buffer by centrifuging at 12 000 rpm for 15 seconds. The column was further washed twice with 500 µL of manufacturer-supplied RPE buffer, centrifuging at 12 000 rpm for 15 seconds and then for 2 minutes. The column was dried by centrifuging at 12 000 rpm for 5 minutes without the lid. CNV RNAs were eluted using 15 µL of RNase-free water into nuclease-free tubes by spinning the column at 14 000 rpm for 1 minute.

2.3 miRNA target analysis

The top 10 miRNAs identified from sequencing were used for analysis. Mature miRNA sequences were downloaded from miRBase. The 3′ untranslated region (UTR) and 5′ UTR sequences of the mouse genome 2020 (GRCm39-2020) were obtained from the UCSC Genome Browser. Target analysis was performed using miRANDA v3.3a with the following parameters: gap open penalty of −9, gap extend penalty of −4, score threshold of 140, energy threshold of −1 kcal mol^{-1}, and scaling parameter of 4. Gene Ontology (GO) analysis of the predicted targets was conducted using the BiNGO tool in Cytoscape v3.9.1. Basic GO annotations were downloaded from geneontology.org, and Bonferroni family-wise error rate correction with a corrected p-value of 0.05 was used to identify overrepresented GO terms.

2.4 Nanoparticle tracking analysis (NTA)

Particle concentration and size distribution of CNVs were determined by nanoparticle tracking analysis using a NanoSight NS300 instrument (Malvern Panalytical, Malvern, UK). The instrument was calibrated with 100 nm polystyrene beads (Thermo Fisher Scientific, Fremont, CA) before use. Samples containing 2 µg of CNVs were diluted up to 1 mL in Milli-Q water, and 1 mL of the diluted sample was loaded into the instrument. The samples were analyzed with a camera level set at 14 and a detection threshold at level 3. Data were processed and analyzed using NTA software version 3.4.

2.5 Zeta potential measurement

The zeta potential of crude CNVs was measured using a Zetasizer Nano ZS (Malvern Instruments Ltd, Malvern, UK), equipped with a laser source at a wavelength of 633 nm and a scattering angle of 13°. The instrument was calibrated according to the manufacturer's instructions by measuring the known surface charge (40 ± 5.8 mV) of 100 nm polystyrene nanoparticles. Samples containing 2 µg of CNVs were diluted up to 1 mL in Milli-Q water or phosphate-buffered saline (PBS), and 800 µL of the diluted sample was loaded into folded capillary cells (DTS 1070 type cuvettes). The zeta potential of each sample was measured three times at 25 °C, with an automatic number of runs and voltage selection after an equilibration time of 120 seconds.

2.6 Transmission electron microscopy (TEM) measurement

For TEM analysis, 2 µL of each sample was deposited on a glow-discharged Formvar/carbon-coated grid, followed by negative staining with 2% uranyl acetate. The samples were examined using a Tecnai G2 Spirit transmission electron microscope (FEI, Eindhoven, The Netherlands). Images were captured with a charge-coupled device camera (Quemesa, Olympus Soft Imaging Solutions GmbH, Münster, Germany).

2.7 *In vitro* digestion of CNVs

Digestive juices, including gastric juice, pancreatic juice, and bile juice, were prepared as previously described (Table S1).[19] To examine whether CNVs survive *in vitro* gastrointestinal conditions, 100 µL of CNVs were mixed with 300 µL of gastric juice and incubated at 37 °C for 120 minutes. Subsequently, 300 µL of pancreatic juice and 150 µL of bile juice were added and incubated at 37 °C for an additional 60 minutes. PBS (replacing the digestive juices) was used as a negative control, undergoing the same *in vitro* digestion steps. Finally, digestive juices were removed by centrifugation at 8 000g at 20 °C for 30 minutes with 3 repetition, and particle and protein concentrations, as well as surface potential of CNVs, were determined by NTA, Qubit assay, and zeta potential measurements, respectively. Morphological changes were examined using TEM. Total phenolic content (TPC), antioxidant activity, and the antioxidant functionality of bioactive associated with CNVs —both pristine and after simulated gastric digestion were also determined. All chemicals and enzymes for the *ex vivo* model system were purchased from Sigma-Aldrich (St Louis, MO, USA).

2.8 Labelling CNVs using lipophilic tracer

After differential centrifugation of CNVs at 2000, 4000, and 15 000g, the supernatant was incubated with 1 mM fluorescent lipophilic tracer DiR (1,1′-dioctadecyl-3,3,3′,3′-tetramethyl-indotricarbocyanine iodide; D12731, Invitrogen, Life Technologies) or DiIC18(7) (1,1′-dioctadecyl-3,3,3′,3′-tetra-methylindotricarbocyanine iodide) at room temperature for 20 minutes. After incubation, the CNVs labeled with DiR or DiIC18, along with DiR- and DiIC18-free controls, were ultra-

centrifuged using a SW28Ti rotor in a Beckman Optima L-100K ultracentrifuge at $100\,000g$ for 2 hours, followed by a washing step at the same speed and duration. To separate the DiR-labeled CNVs from contaminant-free dye, we used gradient ultracentrifugation with OptiPrep™ (Stemcell Technologies, Germany) to collect the fraction containing pure DiR- or DiIC18-labeled CNVs. The dye-labeled EVs or free dye were loaded at the top of a discontinuous OptiPrep solution (5%, 10%, 20%, and 40%) and centrifuged at $100\,000g$ for 16 hours at 4 °C using a Beckman Optima L-100K ultracentrifuge. Fractions containing dye-labeled EVs were collected and used for subsequent experiments.

2.9 Mucopenetration measurement

To determine the penetration of CNVs across the mucin layer, we used a Transwell assay (polyethylene, 1 µm pores, 6.5 mm diameter, providing a surface area of 0.33 cm^2; cellQART, Germany). A 20 µL aliquot of reconstituted mucus (5% mucin) was added to coat the membrane in a well plate and left to settle for 30 minutes. Then, 900 µL of ultrapure water was added to the bottom of the 24-well plates, and 250 µL of CNV solution containing 1×10^{10} particles per mL was gently deposited in the Transwell insert to avoid disturbing and mixing with the mucin layer. The CNVs were incubated with the reconstituted mucus for 24 hours at 37 °C to allow migration through the mucin layer. The percentage of CNVs that traversed the mucin layer in the mucin-coated Transwell was normalized against the amount that passed through the uncoated Transwell, as measured by their fluorescence, using the following formula:

$$\% \text{ particles permeation} = \frac{\text{number of particles through mucus coated membrane}}{\text{number of particles through uncoated membrane}} \times 100\%$$

2.10 Cell culture

Caco-2 cells were maintained in Dulbecco's Modified Eagle's Medium (DMEM; Gibco Life Technology, UK) supplemented with 20% (v/v) fetal bovine serum (FBS; Sigma, USA), 1% (v/v) non-essential amino acids, 1% (v/v) L-glutamine, and 1% penicillin–streptomycin (100 IU mL^{-1}) (Sigma, USA). The cells were incubated at 37 °C in a humidified atmosphere containing 5% CO_2.

2.11 Cytotoxicity and cell proliferation assays

The IncuCyte® Live-Cell Analysis System (Sartorius, UK) was used to assess cytotoxicity, cell viability following H_2O_2 treatment, and the proliferation of Caco-2 cells. Caco-2 cells were seeded at a density of 1×10^5 cells per mL in DMEM supplemented with 20% FBS (100 µL per well) into a 96-well flat-bottom plate and incubated overnight at 37 °C in 5% CO_2. After overnight incubation, the medium was removed, and the cells were washed with PBS before adding fresh medium containing CNV samples. To label dying cells, SYTOX Green nucleic acid stain (diluted 1 : 10 000 in medium) was applied,

causing dying cells to fluoresce green. Cell death was monitored over time, with scans performed every 3 hours at 10× magnification using the standard scanning mode. The IncuCyte® image analysis tools were used to automatically quantify the number of dying cells. All experiments were conducted in triplicate.

2.12 *trans*-Epithelial electrical resistance (TEER) measurement

For the establishment of an *in vitro* cell monolayer, Caco-2 cells were seeded at a density of 1×10^5 cells per mL on cellQART 24-well cell culture inserts (1 µm pore size, PET clear) in a Costar 24-well plate (Corning Costar Corp.). The apical and basolateral compartments of the Transwells were maintained with complete DMEM, which was refreshed every two days. TEER values were measured and recorded using a Millicell ERS-2 resistance system (EMD Millipore Corporation, Burlington, MA). TEER was calculated as follows:

$$\text{TEER} = (R_m - R_i) \times A$$

where R_m is the transmembrane resistance, R_i is the intrinsic resistance of the cell medium, and A is the surface area of the Transwell membrane. TEER was measured every 2–3 days to monitor Caco-2 cell monolayer formation. On day 14 after cell seeding, TEER measurements stabilized, and Caco-2 cell monolayers were used for transport assays.

2.13 CNV transport assays in Caco-2 monolayers

Transport assays were performed following the previous reported method.[20,21] Briefly, cell culture medium was removed, and inserts were transferred to a new 24-well plate. Cells were washed with Hanks' Balanced Salt Solution (HBSS) containing 25 mM HEPES and 4.2 mM $NaHCO_3$ at pH 7.4 for the basolateral side to eliminate residual culture medium, and at pH 6.5 for the apical side to simulate the acidic environment of the small intestine, for 20 minutes at 37 °C. Fluorescently DiIC18-labeled CNVs were diluted in HBSS (pH 6.5) to 1×10^{12} particles per mL and added to the apical compartment. Equal medium levels were maintained in both compartments to avoid hydrostatic pressure effects. Samples from the basolateral acceptor compartment were taken at defined times for cumulative transport studies by measuring the fluorescence signal. TEER was measured before and after each experiment to ensure the integrity of the cell monolayer.

2.14 Cellular uptake assay

DiIC18-labeled CNVs were incubated with Caco-2 cells at 37 °C for 1, 4, and 8 hours. After incubation, the cells were harvested and washed to remove free particles. PKH26 dye (Sigma-Aldrich, USA) was used to stain the cell membrane, and LysoTracker Deep Red (Invitrogen, USA) was used to stain lysosomes in Caco-2 cells. Cell nuclei were visualized by staining with 4′,6-diamidino-2-phenylindole (DAPI; Thermo Fisher Scientific, USA). Images were captured using a confocal microscope (Leica SP8 Falcon, Germany).

2.15 *In vivo* trafficking of CNVs in mice

All animal procedures were conducted at the Laboratory Animal Centre of the University of Oulu (OULAC) in compliance with regulations for the protection of vertebrate animals used for scientific purposes (European Convention Treaty ETS No. 123, European Community Council Directive 2010/63/EU, and Finnish Government Decree 564/2013). The animal experiments were approved by the Finnish National Animal Experiment Board (permit numbers ESAVI/18215/2018 and ESAVI/32696/2023). DiR-labeled CNVs were administered *via* oral gavage to male C57BL/6 mice aged 6–8 weeks and 32 weeks. CNVs were administered at a dose of 100 μL (10 mg kg^{-1}), approximately 1×10^{11} particles per animal. Control animals received 100 μL of PBS saline. For oral gavage administration, mice were fasted for 6 hours prior to the procedure to ensure an empty stomach; water was available *ad libitum*. *In vivo* imaging was performed using the IVIS Spectrum system (PerkinElmer, USA) with an excitation wavelength of 745 nm. Imaging was conducted at time points of 1, 4, 12, and 24 hours after administration of the DiR-labeled CNVs. Mice were anesthetized with isoflurane and imaged for 2–5 minutes. Mice were humanely sacrificed at designated times, and 200–300 μL of blood was collected *via* heart puncture or vena cava sampling. Organs were harvested for *ex vivo* imaging and further examination. To confirm the localization of CNVs at the cellular level in GI tract organs, mice were orally gavaged with 1×10^{11} DiIC18(7)-labeled CNVs and sacrificed 4 and 12 hours later. Plasma was collected from blood samples at different times, diluted in PBS at a 1 : 10 ratio, and pelleted by ultracentrifugation at 100 000g for 2 hours. The pellets were scanned to measure fluorescence intensity using the IVIS Spectrum system (PerkinElmer, USA) with an excitation wavelength of 745 nm. Data were analyzed using Living Image software for IVIS®.

2.16 Immunohistochemistry

Internal organs were excised and fixed overnight in 4% paraformaldehyde (PFA) at 4 °C, then transferred to PBS solution for 24 hours at 4 °C. Samples were dehydrated with 25%, 50%, and 70% ethanol, changing solutions every 24 hours. Tissue sections were embedded in paraffin blocks according to standard procedures and cut into 4–6 μm-thick sections using a microtome, then applied to electrostatically charged microscope slides (*e.g.*, sc-363562). For immunohistochemistry staining, sections were fixed for 10 minutes in 4% formaldehyde (Histolab, Sweden), washed three times for 5 minutes each in PBS, and then blocked using PBS containing 5% goat serum (Life Technologies, Sweden) and 0.3% Triton X-100 (Sigma-Aldrich, Sweden) for 1 hour. The primary antibody (Abcam, Germany) was diluted 1 : 1000 in antibody dilution buffer consisting of PBS with 0.1% Triton X-100 and added to each sample, incubating overnight at 4 °C. Sections were then washed as previously described, and the secondary antibody (Alexa 594 anti-rabbit IgG, Life Technologies) diluted 1 : 500 in antibody dilution buffer was added and incubated for 1 hour at room temperature. Cell nuclei were visualized by staining with DAPI (Thermo Fisher Scientific, USA). Sections were washed again, mounted with coverslips, and imaged using a confocal microscope (Leica SP8 Falcon, Germany).

2.17 Flow cytometry of whole blood

To process 100 μL of whole blood for flow cytometry analysis, 2 mL of room-temperature 1 × 1-Step Fix/Lyse Solution was added, and the tube was gently inverted. The sample was incubated at room temperature, protected from light, for 15 to 60 minutes. An antibody cocktail (concentration 1 : 50), containing fluorophore-labeled primary antibodies for cell-surface markers, was prepared in Flow Cytometry Staining Buffer, protected from light. The antibody cocktail was added to a 100 μL aliquot of whole blood and incubated for 1 hour at 2–8 °C with rotation, keeping it protected from light. Following incubation, samples were washed with 2 mL of Flow Cytometry Staining Buffer. Samples were centrifuged at 500g for 5 minutes at 4 °C, the supernatant was discarded, and the cells were resuspended in 500 μL of Flow Cytometry Staining Buffer. Analysis of the stained immune cells was performed using a FACSCalibur flow cytometer (BD Biosciences, Erembodegem, Belgium). Data were analyzed using FlowJo software v10.8.1 (BD Biosciences).

### 2.18 Quantification and statistical analysis

Experiments were conducted in triplicate unless otherwise noted, and results are reported as mean values with standard deviations. Statistical analysis was performed using one-way analysis of variance (ANOVA) and Tukey's *post hoc* test provided by OriginPro® 2022 (OriginLab Corporation, USA), with statistical significance set at $p < 0.05$.

3. Results and discussion

3.1 Physical properties and RNA content of plant-derived nanovesicles isolated from cloudberry (CNV)

TEM is used to evaluate the size, shape, and vesicular integrity of the PDNVs. The TEM images confirmed the presence of PDNVs in cloudberry juice, revealing their characteristic spherical or cup-shaped structures with lipid bilayer membranous morphology and diameter ranging 60–200 nm (Fig. 1A). Intact PDNVs were observed, showing the preservation of the membrane integrity after isolation using this method. To further assess the size and concentration of these nanovesicles, NTA was conducted. The CNVs displayed a size distribution ranging from 55.1 to 347.4 nm in diameter, with an average diameter of 208.3 ± 10.7 nm and a mode diameter of 170.6 ± 17.1 nm (Fig. 1B). Using the described isolation procedure, the CNV yield was approximately 38.9 ± 18 mg of protein per kg, which was equal to $8.99 \times 10^{12} \pm 2.40 \times 10^{10}$ particles per kg, indicating that cloudberries have a significant potential for large-scale production of PDNVs. This yield level was comparable to other plant sources such as ginger and strawberry and EV isolated from the milk (2–11×10^{12} particles per kg depend on the isolation techniques).[22–24]
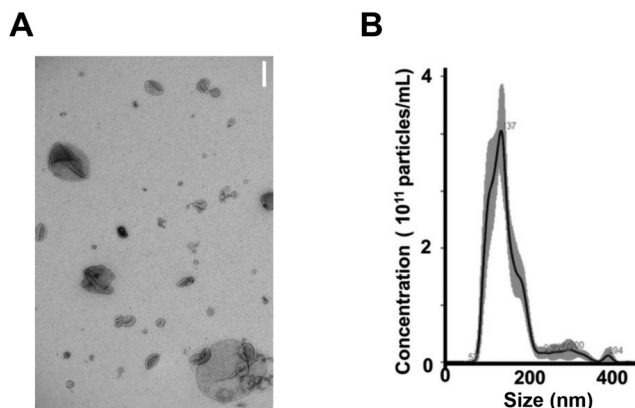
Fig. 1 Morphology and size of CNVs analyzed by (A) transmission electron microscopy (scale bar: 200 nm) and (B) nanoparticle tracking analysis.

Zeta potential measurements indicated that CNVs had a negative zeta potential of −50.6 ± 0.7 mV, similar to values reported in the literature of other plants.[25] Moreover, the purity of isolated CNV using this protocol were estimated using ratio of particle counts to protein concentration, as reported by Webber *et al.*[26] In this regard, an EV-to-protein purity ratio of 3×10^{10} particles per µg of protein is the metric used to qualify a population of EVs as "pure". Herein, the particle-to-protein ratio of purified CNVs was approximately 3.57×10^{10} particles per µg protein, which is considered to be high purity. This is similar values reported for cheries (4×10^{10} particles per µg), Roma tomatoes (3.8×10^{10} particles per µg), and lemon citrus (1×10^{10} particles per µg).[27,28] TEM images (Fig. 1A) and NTA data (Fig. 1B) together show that CNVs display a degree of size and shape heterogeneity, ranging from ~60 nm to over 200 nm in TEM and 55–347 nm in NTA. Such heterogeneity is consistent with reports on PDNVs from grapes, ginger, and citrus, and likely reflects vesicles originat-
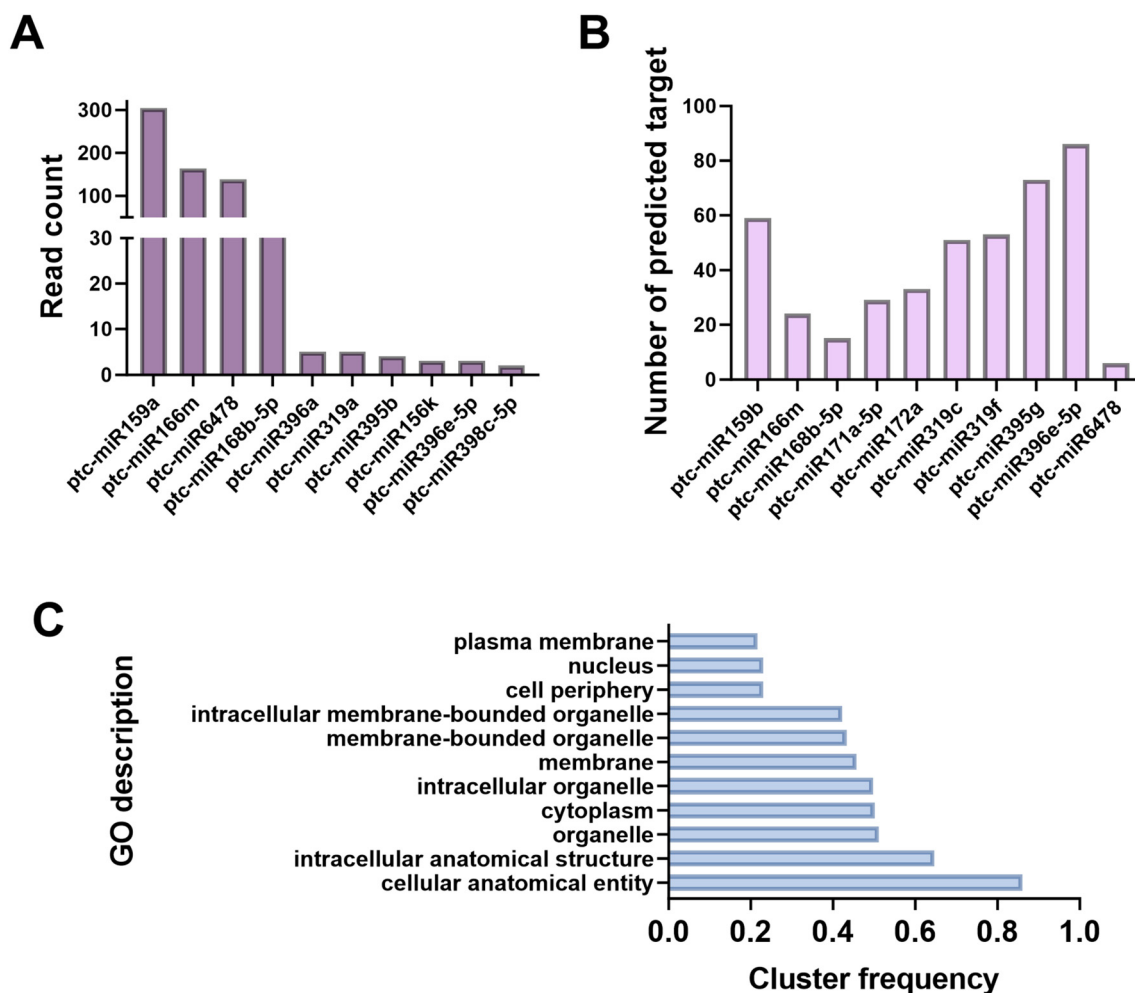
Fig. 2 (A) Analysis of the top 10 miRNA profiles in CNVs. (B) Number of predicted mouse gene targets for CNV miRNAs identified using miRANDA v3.3a with parameters: gap open penalty of −9, gap extend penalty of −4, score threshold of 140, energy threshold of −1 kcal mol⁻¹, and scaling parameter of 4. (C) Gene Ontology (GO) annotation of the predicted target genes performed using Cytoscape 3.9.1 with basic GO annotation.

ing from multiple plant cell types and subcellular compartments. Importantly, despite this variation, the majority of vesicles retain intact bilayer morphology and negative zeta potential, supporting their stability and functionality in subsequent mucus penetration, epithelial transport, and *in vivo* biodistribution assays.

CNVs are enriched with miRNAs—small, endogenously derived 18–25 nt RNAs that may regulate gene expression and cellular communication. Due to the limited availability of cloudberry genomic data, we aligned sequenced reads to the *Populus trichocarpa* genome to identify noncoding RNAs. The top 10 most abundant miRNAs (Fig. 2A) were further analyzed for potential interactions with mouse genes using miRanda v3.3a. Notably, miR159, 166, 168, and 396 were among the most 10 abundant miRNAs detected, consistent with previous reports on PDNVs.[29] The number of predicted target genes and Gene Ontology (GO) analysis (Fig. 1C and D) suggest that these miRNAs may influence a wide range of cellular processes, including structural, metabolic, and signaling pathways. Notably, miR396, miR159, miR168, and miR166 have been previously reported to target mammalian genes related to inflammation pathways (*e.g.*, cytokines and NF-κB signaling components), oxidative stress, and apoptosis.[29–31] These predictions are supported by our *in vitro* anti-inflammatory assays in THP-1 cells, which measured IL-1β mRNA expression using qPCR under both LPS-stimulated and unstimulated conditions (Fig. S2). CNVs alone did not induce IL-1β expression, indicating that they do not trigger an inflammatory response at the tested dose (50 μg mL^{-1}). However, co-incubation of CNVs with LPS (10 ng mL^{-1}) significantly reduced IL-1β expression compared to LPS treatment alone. These results suggest that CNVs may exert functional effects in recipient mammalian cells through miRNA-mediated modulation of inflammatory gene expression.

3.2 Stability of CNV in gastrointestinal solution

One obstacle in utilizing orally administered CNVs for therapeutic applications is their insufficient stability within the GI tract and limited ability to be effectively absorbed into the bloodstream. CNVs must sequentially overcome both mucus and epithelial barriers. The GI tract is coated with mucus, which protects the organs by maintaining their integrity against foreign substances. As the initial defense mechanism, the mucosal layers prevent the adherence of foreign pathogens and particles and promote their clearance through the cycling mucus.[32] The mucin particles had an average diameter of 268.7 ± 16.9 nm, consistent with sizes reported by others.[33] These particles featuring hydrophobic cysteine-rich domains and negatively charged sialic acid within the mucus. Intestinal mucus, which is a constantly renewing and slippery secretion, can quickly trap and eliminate foreign particles, especially those with cationic and hydrophobic surface properties.[34] Effective diffusion of CNVs through the mucus requires minimal interactions between the CNVs and mucin particles.
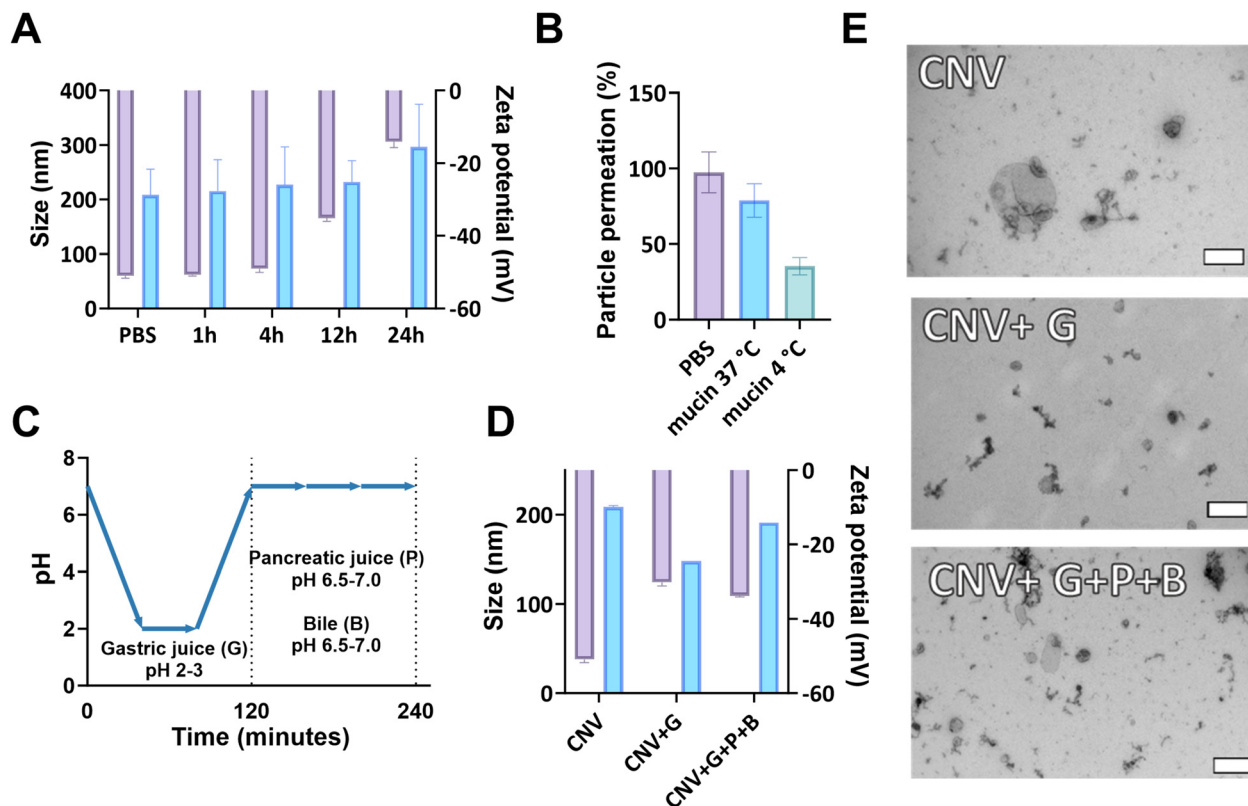
We examined the interaction between CNVs and mucus (5% mucin solution) over time by measuring changes in their size and surface charge. The CNVs exhibited minimal size increase and maintained a highly negative surface charge for up to 12 hours (Fig. 3A), suggesting no significant aggregation. After 24 hours, a slight increase (∼1.5-fold) in particle size and a decrease in negative surface charge indicated potential interactions with mucin particles. To determine the penetration of CNVs across the mucin layer, we used a Transwell assay with a 1 μm pore-size filter lined with a mucin layer. Fluorescent CNVs collected from the basal chamber after 12 hours of incubation were measured and compared to freely diffusing fluorescent CNVs without the mucin layer. We observed minimal interaction between CNVs and mucin particles in reconstituted mucus, resulting in efficient penetration of CNVs through the mucin layer in the Transwell assay (Fig. 3B). This high mucopenetration is likely due to the small size (less than 200 nm) and negatively charged, hydrophilic nature of CNVs. Both CNVs and mucin carry strong negative surface charges, causing electrostatic repulsion that limits direct interactions in the absence of bridging ions such as Ca^{2+}, thereby facilitating freer particle movement.[35] Nevertheless, weak transient interactions may occur *via* hydrogen bonding (*e.g.*, between hydroxyl and carboxyl groups), van der Waals forces, and limited hydrophobic interactions, leading to partial mucoadhesion and short-term retention. Additionally, the naturally high pectin content of CNVs may contribute to mucin binding through polymer entanglement.[36,37] Adsorption of mucin or luminal proteins onto the vesicle surface may further lead to the formation of a mucin-associated corona, dynamically modulating surface characteristics and enhancing residence time within the gastrointestinal mucus layer.

Before CNVs can reach the intestinal epithelial barrier, they must navigate the stomach and intestinal lumen, which are characterized by varying pH levels, ionic strengths, and complex mixtures of digestive fluids and food molecules.[38] It has been reported that milk-derived EVs can endure very low pH, high temperatures, and freezing/thawing procedures in enzyme-free *in vitro* systems. They also withstand the harsh conditions of the gastrointestinal tract, as demonstrated by both *in vitro* and *in vivo* studies using fluorophore-labeled EVs. However, there is a limit information on the behavior of PDNVs.[39,40] To investigate the resilience of CNVs against digestive juices, we created an *in vitro* digestive system simulating the gastrointestinal environment, adapted from Kopf-Bolanz *et al.*[19] This system uses buffers that mimic different digestive fluids: gastric juice (G) with pepsin at pH 2–3, pancreatic juice (P) with pancreatin at pH 6.5–7, and bile juice (B) with bile acids at pH 6.5 (Fig. 3C). To investigate the evolution of CNVs after incubation with each digestive enzyme, we characterized the morphologies, sizes, and surface charge changes of the CNV–protein complexes by TEM, NTA, and zeta potential measurements (Fig. 3D and E, Table 1, and Fig. S3 in SI).

TEM analysis indicated that CNVs maintained a relatively stable structure after exposure to the gastric solution, preserving their original lipid bilayer morphology, although their number slightly decreased. The surface charge of CNVs became slightly less negative (−30 mV) compared to their

Fig. 3 (A) Interaction between CNVs and mucin particles after incubation in reconstituted mucus for 1, 4, 12, and 24 hours at 37 °C, as indicated by changes in average size and surface zeta potential. (B) Mucopenetration of CNVs across a mucin layer in a Transwell assay for 12 hours at 37 °C and 4 °C, showing the percentage of CNVs that passed through the mucin layer on top of a 1 μm pore-size membrane relative to a Transwell without the mucin layer. (C) Schematic diagram of CNV treatment in an *in vitro* digestive system. (D) Zeta potential and size distribution, and (E) morphology of CNVs before and after undergoing *in vitro* digestion (scale bar: 200 nm). Three independent experiments were performed. Abbreviations: CNV, cloudberry nanovesicles; G, gut solution; G + P + B, gut, pancreas, and bile solutions.

Table 1 Summary of physical properties of CNVs after GI solution treatment

Sample	Protein concentration ($\mu g \, mL^{-1}$)	Particle concentration (particle per mL)	Nanoparticle (μg protein)	Size (nm)	Zeta potential (mV)
NV	13.4	4.78×10^{11}	3.57×10^{10}	208.3 ± 10.4	-50.6 ± 0.7
NV + G	10.3	3.70×10^{11}	3.59×10^{10}	147.8 ± 59.7	-30.1 ± 0.8
NV + G + P + B	12.9	2.05×10^{11}	1.58×10^{10}	191.1 ± 89.4	-33.7 ± 0.5

Abbreviations: NV, native cloudberry nanovesicles; G, gastric juice; P, pancreatic juice; B, bile juice.

pristine state (−50 mV), likely due to the pH conditions; yet, no significant aggregation was observed. The average size of CNVs decreased from 200 nm to 138 ± 5 nm after digestion in gastric juice. Additionally, 22% of the particles and 31% of the protein were lost during either the digestive process in the gastric solution or the subsequent washing step. In contrast, after pancreatic and bile juice treatment, despite the lower number of particles, the protein concentration increased compared to that after gastric solution treatment. This size reduction of CNVs agrees with previous reports on milk, carrot, and grapefruit-derived NVs;[22,40,41] however, it contrasts with NVs isolated from edible tea flower and ginseng.[42,43]

Following treatment with pancreatic and bile juices, both TEM and NTA confirmed an increase in particle size compared to post-gastric juice treatment, likely due to the formation of an outer layer around the CNVs' surface (protein corona), composed of intestinal proteins and peptides and possible slightly aggregate. Despite the different pH environments, the surface charge remained similar to the post-gastric treatment, probably due to the charge characteristics of the protein corona affecting the net surface potential of CNVs.[44] Although different pH levels can alter the size and zeta potential of CNVs, they remain nanoscale in size, exhibit good stability, and their surface potential changes are consistent with their

natural properties. These findings suggest that CNVs are resilient in the GI environment, maintaining their nanoscale size and structural integrity. PDNVs derived from sources such as ginger, grapefruit, and broccoli have been shown to exhibit greater stability under harsh gastrointestinal conditions compared to synthetic nanoparticles or mammalian EVs. This enhanced stability is likely due to their unique lipid compositions—including glycerolipids and phospholipids—as well as stabilizing components like associated proteins and polysaccharides.[45] In the case of CNV, the naturally high pectin content may further contribute to gastric protection by buffering stomach acid and delaying gastric emptying, thereby enhancing NV stability.[36,37] The structural stability of CNVs under GI conditions is further supported by (i) TEM and NTA analyses (Fig. 3D, E and Table 1) showing preserved nanoscale size, bilayer morphology, and negative surface charge after gastric, pancreatic, and bile treatments; (ii) DiO-label fluorescence stability and morphology data (Fig. S5), indicating minimal membrane disruption after digestion; and (iii) single-particle tracking analyses (Fig. S6) showing maintained motion profiles post-digestion. To emphasize the relative resilience of CNVs, we compared digestion-treated CNVs with CNVs subjected to heat and sonication (Fig. S10), where the latter exhibited clear bilayer collapse and vesicle fragmentation. Together, these data provide direct experimental evidence that CNV stability is not only an inferred property based on composition (lipids, pectin, protein corona) but is demonstrable under simulated GI conditions. These findings are consistent with previous reports showing that PDNVs from *Catharanthus roseus* leaves,[46] turmeric,[47] and *Camellia sinensis*[42] remain stable in simulated gastric fluids (pH 2.0) and intestinal fluids (pH 6.5).

3.3 Bioactivity and *in vitro* study of pristine and gut-treated CNV

One of the key challenges for orally delivered NVs is their ability to cross the intestinal epithelium. To assess this, we evaluated the ability of CNVs to enter and pass through the epithelium. Efficient cell internalization of CNVs is a prerequisite for exerting their bioactivity. To assess the functional integrity of CNVs after digestion, we examined their cellular uptake, ability to traverse the epithelial barrier, and bioactivity using human intestinal epithelial (Caco-2) cells.[48]

Nanosized materials may traverse cellular barriers *via* paracellular or transcellular routes. The paracellular route involves passage between epithelial cells through transient disruption of tight junctions, while the transcellular route involves internalization, endocytosis, transport across the cell body, and secretion at the opposite cell surface (transcytosis).[49] TEER measurements were used to quantitatively assess the integrity of epithelial cell monolayers, which is influenced by tight junction dynamics.[50] In our assays, Caco-2 cells were cultured on Transwell inserts, with TEER measurements taken every 3 days. On day 14 post-seeding, TEER values stabilized at 1749 Ω cm^2 ± 72 Ω cm^2, and the monolayers were used for transcytosis assays (Fig. S4).

To study the uptake of CNVs, DiO18-labeled CNVs were incubated with Caco-2 cell monolayers in the upper chamber. The stability of fluorescence signals and morphology of DiO18-labeled CNVs after digestion was confirmed by spectrofluorometric analysis and TEM, respectively (Fig S5). Cellular uptake was monitored at 1, 4, and 8 hours using confocal microscopy (Fig. 4A, left), and individual CNVs were tracked using single-particle tracking (Fig. S6). The digested CNVs were rapidly taken up by Caco-2 cells within 1 hour, and internalization increased over time, likely due to the protein corona (*e.g.*, bile proteins) facilitating uptake. Moreover, orthogonal views of cell images showed that the CNVs were not only present on the cell surface but also found in the basal part of the cells (Fig. 3B, left). After 8 hours, both pristine and gut-treated CNVs were internalized by Caco-2 cells and mostly colocalized with lysosomes (Fig. S7 in SI).

Transport across the Caco-2 monolayer is a Food and Drug Administration (FDA) and European Medicines Agency (EMA)-approved method to estimate drug permeability *in vitro*.[51] For CNV permeability assays, fluorescence in the lower chamber medium was measured at various time points (Fig. 3B, right). Fluorescence was first detected at 120 minutes, with intensity increasing by 43% and 25% at 240 minutes for pristine and digested CNVs, respectively. Transwells without cells served as controls for passive diffusion, with fluorescence detected after 5 minutes and stabilizing after 60 minutes. To estimate NV permeability efficiency, we compared fluorescence units recovered in the lower chamber to those in the upper chamber. Of the 5010 fluorescence arbitrary units (approximately 5 × 10^9 NVs) seeded, 20% ± 2% passed through the epithelial monolayer at 120 minutes, and 29% ± 13% at 240 minutes. For digested CNVs, efficiency slightly decreased, which may be due to some of the CNVs being entrapped in cellular organelles within endocytic or transcytotic pathways, or undergoing lysosomal degradation. The integrity of the monolayer was monitored by TEER measurements before and after the experiment. Throughout the 8-hour CNV incubation, TEER values remained constant at 1730 Ω cm^2 ± 84 Ω cm^2, indicating no impact on cell monolayer integrity.[20,52]

Moreover, given that CNVs maintained their morphology, size, and quantity in the simulated digestive system, we also investigated whether their bioactivities were compromised by gastrointestinal digestion. To evaluate the functional stability and bioactivity of CNVs following oral administration, we first assessed the effects of simulated gastric digestion. The presence of miR159 and miR166 in both pristine and digested CNVs was confirmed by qPCR (Fig. 5A). Since the aim was to verify the presence of plant-derived miRNAs rather than quantify their relative abundance, no normalization was applied. An increase in *Cq* values for miR159 (from ~28 to ~31) was observed, indicating partial degradation during digestion. In contrast, miR166, which was present at lower levels even in pristine CNVs, showed minimal change in Ct values after digestion. These results indicate that although miR159 undergoes some degradation, its detectability after digestion reflects partial retention of functional stability. This may be attributed
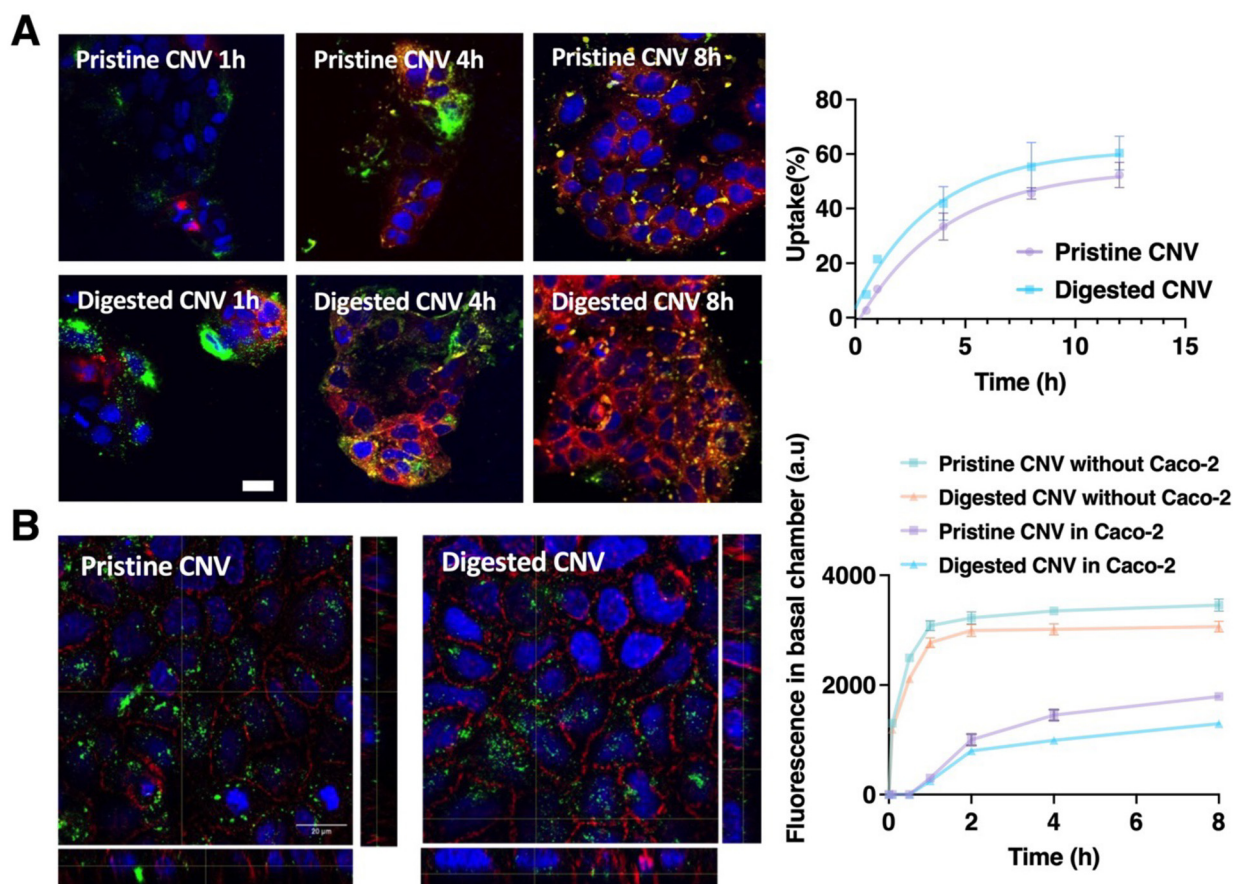
Fig. 4 (A) Time-dependent uptake of CNVs by Caco-2 cells. Confocal microscopy images display the uptake of pristine and digested CNVs by Caco-2 cells (CNVs in green, nuclei in blue, cell membranes in red); scale bar: 20 μm. The uptake of pristine and digested CNVs by Caco-2 cells over time is quantified ($n = 3$), fitted with exponential decay ($R^2 = 0.99$). (B) Transport efficiency of CNVs across Caco-2 monolayers. Orthogonal views of pristine and digested CNVs within Caco-2 cell monolayers are shown; scale bar: 20 μm. Fluorescence measurements in the lower chamber medium indicate the extent to which CNVs have traversed the Caco-2 cell monolayers.

to plant miRNAs possess a 2-O-methyl modification at their 3-ends, which enhances their resistance to enzymatic degradation and uridylation, supporting their stability in harsh gastrointestinal environments.[51,52]

CNVs, rich in polyphenols, were assessed for total phenolic content (TPC) and antioxidant capacity using the Folin–Ciocalteu and DPPH (2,2-diphenyl-1-picrylhydrazyl) assays (Fig. 5A, B and Fig. S8), respectively.[53]Although digestion moderately reduced TPC and antioxidant activity, CNVs retained their ability to protect cells from H_2O_2-induced oxidative stress, indicating preserved antioxidant functionality (Fig. 5C). This resilience may be due to the stable lipid membrane of CNVs, which protects bioactive compounds. Additionally, polyphenols are known for their stability in acidic environments, helping retain their bioactivity after digestion.[54]

Cell proliferation plays a pivotal role in tissue healing.[53] The toxicity and proliferation effects of both pristine and digested CNVs were measured using Sytox dyes in an IncuCyte system. Pristine CNVs displayed enhanced proliferation of Caco-2 cells compared to the control, which is similar to other PDNVs from sources such as aloe vera, apple, ginger, and

grape.[54–56] Digested CNVs did not significantly affect cell viability at the tested concentrations (protein concentration 5 μg) but slightly reduced the proliferation effect, though it remained significantly different from the control. These findings indicate that although the GI environment impacts NVs, CNVs retain their structure and function.

3.4 *In vivo* study of CNV exposure in mice of different ages

The *in vivo* biodistribution and safety of CNVs were evaluated in animal models, particularly in young and old mice. Intestinal mucus, a physically cross-linked hydrogel, significantly influences particle penetration based on particle size. Most CNVs are nanosized, which is crucial since the mucus layer is highly effective at immobilizing and removing cationic and hydrophobic molecules and particles. To assess systemic distribution, we administered CNVs labeled with an infrared fluorescent membrane dye (DiR) *via* gavage. DiR intensely fluoresces only when integrated into a lipid membrane, making it ideal for *in vivo* applications due to its high tissue penetrance and low autofluorescence.[57] After labeling CNVs with DiR, NTA and EM (Fig. S9) confirmed that a typical circular
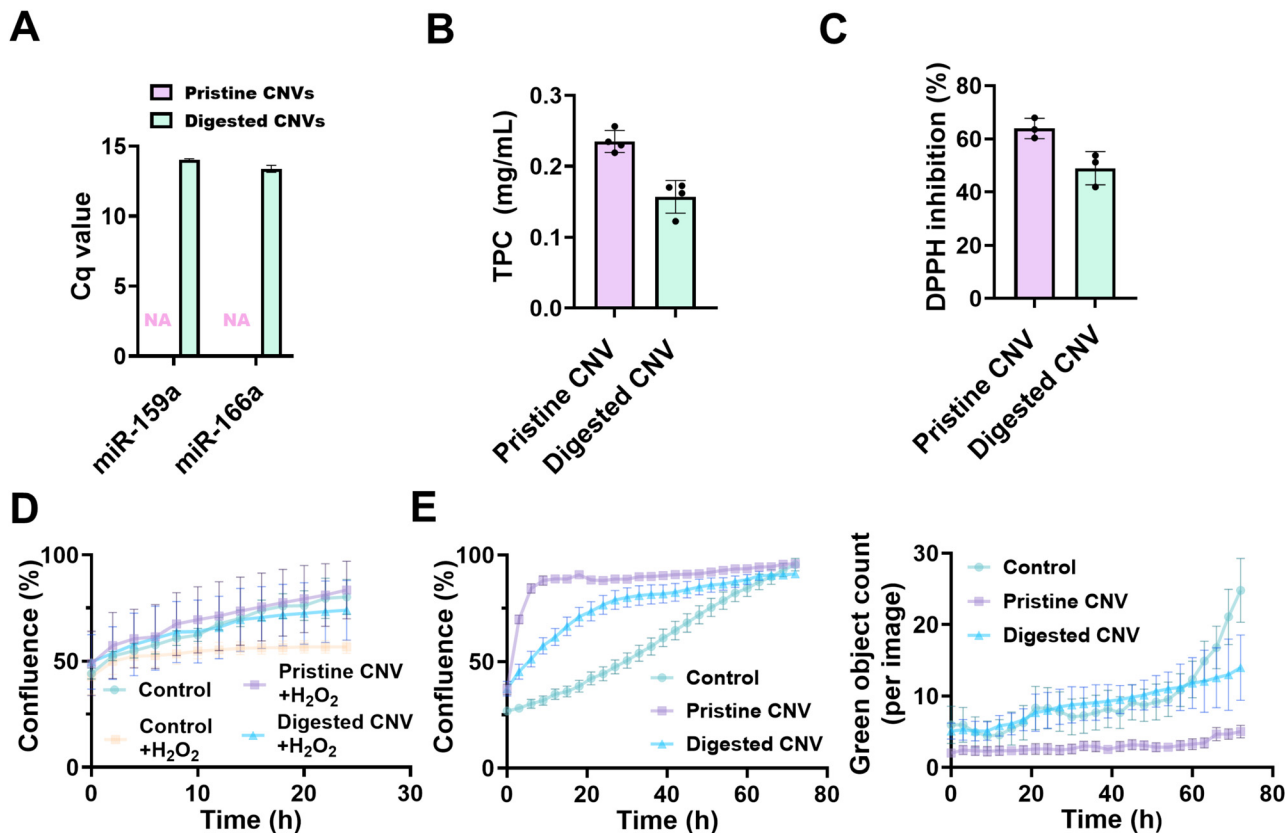
Fig. 5 Bioactive components and antioxidant functionality of pristine and digested CNVs. (A) Detection of miR159 and miR166 in pristine and digested CNV by quantitative PCR. The results are presented as the *Cq* values. (B) Total polyphenol content (TPC) was quantified from equal amounts of pristine and digested CNVs using the Folin–Ciocalteu assay, with results expressed relative to a gallic acid standard curve. (C) Antioxidant activity of equal amounts of pristine and digested CNVs was measured using the DPPH radical scavenging assay. (D) Antioxidant functionality was evaluated by assessing the protective effect of 5 μg protein-equivalent CNVs (pristine and digested) against H_2O_2-induced oxidative stress in Caco-2 cells. (E) Effects of CNVs on the proliferation and viability of Caco-2 cells over 3 days, as measured by IncuCyte®, illustrating the impact of pristine and digested CNVs.

lipid bilayer structure was present in the solution. NTA data showed a similar size with an average diameter of 200 nm, indicating that DiR labeling did not affect vesicle morphology.

Several studies have demonstrated that the route of administration can affect the biodistribution of EVs. Intravenous (IV) injection typically results in a predominant accumulation of EVs in the liver (over 60%), while intraperitoneal (IP) and subcutaneous (SC) injections favor distribution to the pancreas (more than 10%) and gastrointestinal (GI) tract (over 35%). Oral gavage (OG) leads to greater than 50% accumulation in the GI tract, indicating that oral administration is particularly advantageous for targeting treatments related to gut health.[22,58] Live mice were imaged at 1, 4, 12, and 24 hours after oral gavage using an *in vivo* imaging system (IVIS) to assess biodistribution. To confirm that the fluorescent signal originated from DiR-labeled CNVs and not from free dye, PBS without CNVs was incubated with DiR and subjected to ultracentrifugation as a control. The control solution, when administered to the mice, showed no signal (Fig. S8), confirming that the fluorescence from treated mice was from labeled

CNVs. Fluorescent whole-mouse imaging (Fig. 6A) showed increasing signals over time, peaking at 4 hours in young mice and 12 hours in older mice, which is significantly different compared to the control.

After this peak, the signal gradually decreased for young mice, likely due to clearance from the body, while a similar signal was observed even after 24 hours in older mice. However, whole-body imaging did not provide sufficient accuracy to determine the tissue origin of the signal. Therefore, to minimize signal interference, organs were harvested and imaged *ex vivo* (Fig. 6B).

The results showed higher fluorescence in elderly mice compared to young mice. This difference can be attributed to the 20–25% reduction in gastric acid secretion with age, which increases gastric pH.[59,60] The higher pH reduces CNV degradation, leading to a stronger fluorescence signal in older mice. Imaging revealed that between 4 and 12 hours, the fluorescence was mostly detectable in the GI tract and decreased over a 24-hour period for both young and old mice. In young mice, CNVs rapidly passed through the stomach and started
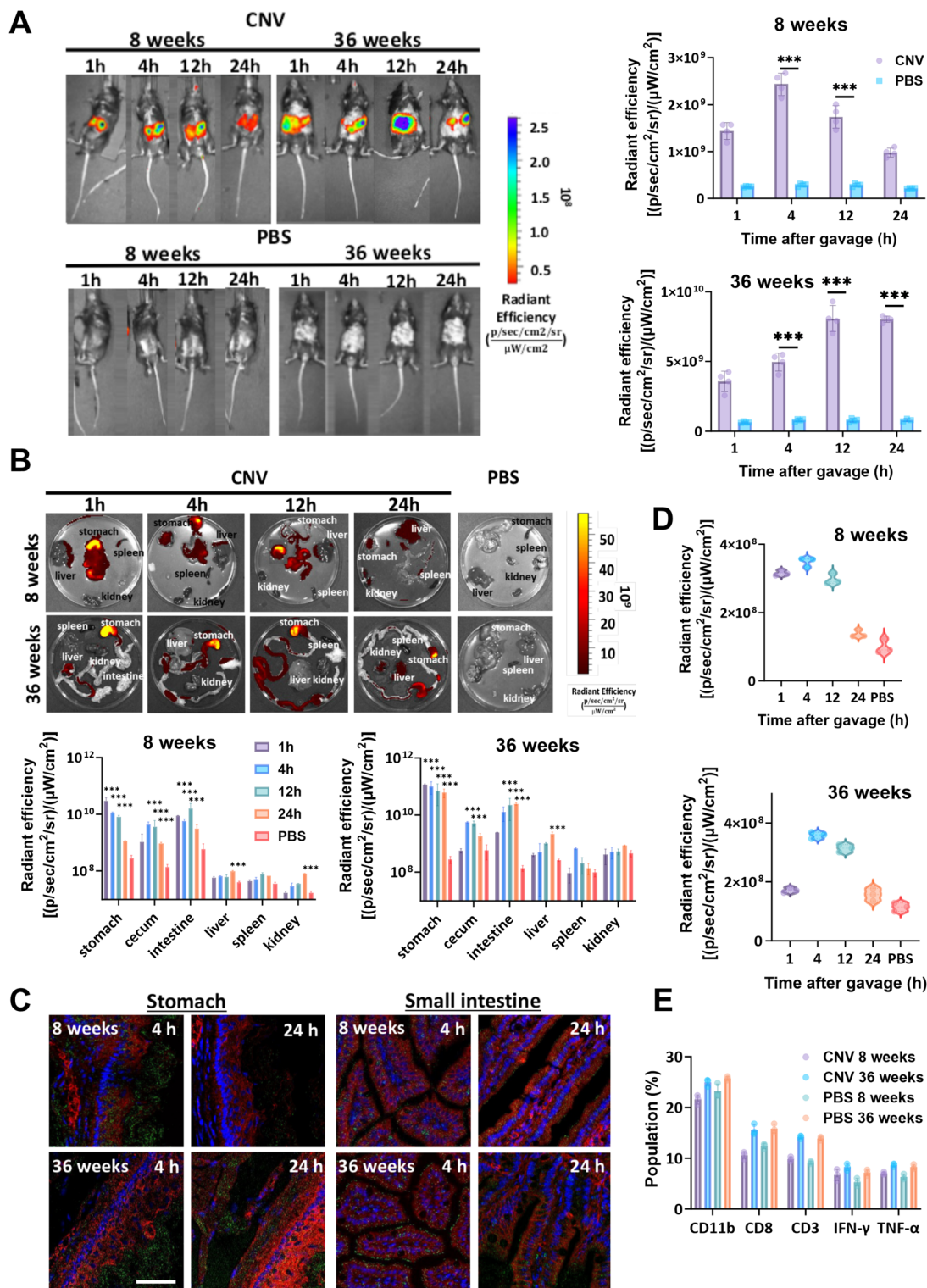
Fig. 6 (A) Whole-body *in vivo* imaging of CNV trafficking. C57BL/6 mice were administered DiR dye-labeled CNVs *via* oral gavage and imaged at 1, 4, 12, and 24 hours post-administration. The left panel shows representative *in vivo* images, and the right panel presents a graph of mean fluorescent signal (radiant efficiency) across the whole body (*n* = 3). (B) Organ-specific biodistribution. Representative IVIS images of harvested organs at 1, 4, 12, and 24 hours post-oral gavage are shown in the left panel. The right panel displays quantification of mean fluorescence (radiant efficiency) in each organ (*n* = 3). (C) Immunofluorescence analysis of CNV (green) absorption in tissues. Representative images of stomach and intestine sections collected at 4 and 24 hours post-gavage, immunostained for tight junction protein ZO-1 (red) and nuclei (DAPI, blue), with CNVs detected in the green channel. Scale bar: 50 μm. (D) Serum fluorescence analysis. DiR fluorescence in serum was quantified at 1, 4, 12, and 24 hours following CNV administration. (E) Immune response to short-term CNV exposure. Expression of immune-related protein markers in blood was assessed 24 hours after oral gavage of CNVs.

accumulating in the duodenum–ileum of the small intestine, colon, and cecum within 1 hour, while older mice showed later accumulation, with the highest fluorescence in the intestine occurring at 12 hours. After 12 hours of oral administration, large amounts of CNVs were still visible in the stomach of older mice. After 24 hours, the CNV signal subsided significantly in most GI tract organs for younger mice, while strong signals remained in older mice, indicating slower absorption, which may relate to reductions in gut motility and changes in gastric pH. At 24 hours, fluorescence was also observed in the liver, spleen, and kidney for both age groups. CNVs migrating from the gut to the liver might do so *via* vascular vessels and can spread through the liver's vascular system.[61]

To better understand the absorption of CNVs in the GI tract, we evaluated the distribution of CNVs in the stomach and intestinal tissues at 4 and 24 hours post-oral administration using confocal microscopy analysis (Fig. 6C). After 4 hours, most CNVs were still present in the stomach in both age groups. This finding aligns with organ imaging results, which also revealed a high quantity of CNVs in the stomach tissue of older mice even after 24 hours. The presence of CNVs in the small intestine was confirmed by confocal immuno-staining for the tight junction protein ZO-1 (Fig. 6C). Fluorescence imaging of intestinal sections indicated that at 4 hours, CNVs were primarily distributed around the villi in the small intestine (jejunum and ileum), with a higher concentration of CNVs in young mice. The co-localization of ZO-1 and CNVs in gut epithelia within 4 hours suggests that orally delivered CNVs are absorbed through the enterocytes of the small intestine in both age groups. By 24 hours post-administration, the fluorescence intensity of CNVs had markedly decreased. To further determine how much CNV enters the peripheral blood, circulating CNVs were isolated from the serum using a standard protocol. The results indicate that circulating CNVs were detected 1 hour after mice were gavaged with CNVs in younger mice and a bit later for the older ones, reaching a peak at 4 hours and then essentially returning to a basal level 24 hours after gavaging (Fig. 6D). This result confirmed that aging contributes to delayed absorption into the bloodstream without significantly altering overall absorption.[62,63]

To assess the immune effects of short-term CNV treatment, we measured changes in immune system levels in the blood (Fig. 6E). The immune system comprises various cells and molecules, including innate immune cells (macrophages, dendritic cells, natural killer cells, neutrophils, and mast cells) and adaptive immune cells (T cells and B cells). Key immune molecules include cytokines, adhesion molecules, immunoglobulins, and the complement cascade. CD8 and IFN-γ are markers for activated $CD8^+$ T cells, which are crucial for the immune response to viral or intracellular infectious agents, antitumor immunity, and immune surveillance.[64] CD11b regulates leukocyte adhesion and migration, mediating the inflammatory response. The balance between pro-inflammatory and anti-inflammatory cytokines is vital for modulating inflam-

mation. Pro-inflammatory cytokines such as TNF-α, IL-1β, and IL-6 play key roles, with TNF-α being primarily secreted by macrophages and involved in neutrophil activation, tumor necrosis, and stimulation of adhesion molecules. Our results showed no significant increase in the population of immune cells in the blood 24 hours post-treatment with CNVs, as indicated by no significant changes in the CD8, CD11b, and IFN-γ protein markers. However, there was a tendency toward higher TNF-α levels in the older mice group compared to the younger group. Aging affects phagocytic cells of the macrophages and complement pathways. Macrophages have increased cell numbers, reduced phagocytic capacity, but increased production of cytokines such as TNF-α, IL-1β, and IL-6.[65] Nevertheless, no significant increase in TNF-α was observed in either age group 24 hours after administering CNVs. These findings align with our *in vitro* THP-1 data (Fig S9) and others,[25,56,66] where CNVs alone did not elevate IL-1β, but co-treatment with LPS reduced inflammatory cytokine levels, confirming their context-dependent immunomodulatory role. These results support the safety of CNVs, showing no systemic inflammation, efficient gastrointestinal transit, and blood absorption. Importantly, the physiological state of the host may influence the therapeutic potential of NVs.

4. Conclusion

This comprehensive study highlights the unique physical properties, biomolecular content, and potential for mass isolation of PDNVs from cloudberries. Our findings confirm that CNVs not only withstand GI digestion but also exhibit favorable biodistribution patterns, prolonged retention in the GI tract, efficient cellular uptake, effective intestinal barrier crossing, successful transfer into the bloodstream, and low immunogenicity. Therefore, CNVs represent promising, stable oral delivery vehicles suitable for both young and elderly mice. Future research should aim to elucidate the specific mechanisms of CNV interaction with target cells, optimize delivery methods, and validate their therapeutic efficacy in relevant disease models.

Author contributions

F. W. P. and K. B. S.: conceptualization (lead), data curation (equal), formal analysis (lead), investigation (lead), methodology (lead), visualization (lead), writing – original draft (lead), writing – review and editing (lead). F. N., R. M, and M. S.: data curation (equal), formal analysis (equal), methodology (equal), writing – original draft (equal), writing – review and editing (equal). S. W.: visualization (equal), supervision (equal), conceptualization (equal), writing review and editing (equal). S. K: methodology (supporting), project administration (lead). A. S.: methodology (supporting). S. J.-L., C. E. and H. L.: funding acquisition (equal), supervision (equal), writing review and editing (equal). S. J. V.: funding acquisition (lead), supervision

(lead), conceptualization (equal), writing review and editing (equal). The manuscript was written through the contributions of all authors. All authors have approved the final version of the manuscript.

Conflicts of interest

The authors declare no competing financial interest.

Data availability

All data supporting the findings of this study are available within the article and its SI. No additional datasets were deposited in public repositories. The Supplementary Information includes experimental methods, additional fig. (S1–S10) on nanovesicle characterization, stability, transcytosis, and bio-distribution, and Table S1 with digestive juice compositions. See DOI: **https://doi.org/10.1039/d4nr04694c**.

Acknowledgements

References

1 T. Gooch, in *The Stanford Encyclopedia of Philosophy*, ed. E. N. Zalta and U. Nodelman, Metaphysics Research Lab, Stanford University, Fall, Ludwig Andreas Feuerbach, 2023, **https://plato.stanford.edu/archives/fall2023/entries/ludwig-feuerbach/**.

2 J. Yang, L. M. Farmer, A. A. A. Agyekum and K. D. Hirschi, *Cell Res.*, 2015, **25**, 517–520.

3 X. Wang, M. Zhang, S. R. L. Flores, R. R. Woloshun, C. Yang, L. Yin, P. Xiang, X. Xu, M. D. Garrick, S. Vidyasagar, D. Merlin and J. F. Collins, *Mol. Ther.*, 2019, **27**, 493–506.

4 E. Berger, P. Colosetti, A. Jalabert, E. Meugnier, O. P. B. Wiklander, J. Jouhet, E. Errazurig-Cerda, S. Chanon, D. Gupta, G. J. P. Rautureau, A. Geloen, S. El-Andaloussi, B. Panthu, J. Rieusset and S. Rome, *Mol. Ther. – Methods Clin. Dev.*, 2020, **18**, 880–892.

5 J.-H. Hwang, Y.-S. Park, H.-S. Kim, D.-h. Kim, S.-H. Lee, C.-H. Lee, S.-H. Lee, J.-E. Kim, S. Lee, H. M. Kim, H.-W. Kim, J. Kim, W. Seo, H.-J. Kwon, B.-J. Song, D.-K. Kim, M.-C. Baek and Y.-E. Cho, *J. Controlled Release*, 2023, **355**, 184–198.

6 D. Fujita, T. Arai, H. Komori, Y. Shirasaki, T. Wakayama, T. Nakanishi and I. Tamai, *Mol. Pharm.*, 2018, **15**, 5772–5780.

7 S. Usui, Q. Zhu, H. Komori, Y. Iwamoto, T. Nishiuchi, Y. Shirasaka and I. Tamai, *Drug Metab. Pharmacokinet.*, 2023, **52**, 100512.

8 F. W. Pratiwi, R. T. Thomas, M. Karzarjeddi, M. Sarpola, I. Miinalainen, O. Makieieva, S. Jokipii-Lukkari, C. Elbuken, K. Oksman, S. J. Vainio and H. Liimatainen, *Biomacromolecules*, 2024, **25**, 5847–5859.

9 K.-J. Lo, M.-H. Wang, C.-T. Ho and M.-H. Pan, *J. Agric. Food Chem.*, 2024, **72**, 2853–2878.

10 N. J. Hunt, P. A. G. McCourt, Z. Kuncic, D. G. Le Couteur and V. C. Cogger, *Front. Nanotechnol.*, 2022, **4**, 832524.

11 S. N. Hilmer, *Expert Opin. Drug Metab. Toxicol.*, 2008, **4**, 1321–1331.

12 T. S. Ghosh, F. Shanahan and P. W. O'Toole, *Nat. Rev. Gastroenterol. Hepatol.*, 2022, **19**, 565–584.

13 M. Gandhi, D. V. Glidden, K. Mayer, M. Schechter, S. Buchbinder, B. Grinsztejn, S. Hosek, M. Casapia, J. Guanira, L. G. Bekker, A. Louie, H. Horng, L. Z. Benet, A. Liu and R. M. Grant, *Lancet HIV*, 2016, **3**, e521–e528.

14 Z. Fang and K. Liu, *J. Controlled Release*, 2022, **350**, 389–400.

15 X. Zhang, G. Chen, H. Zhang, L. Shang and Y. Zhao, *Nat. Rev. Bioeng.*, 2023, **1**, 208–225.

16 Y. Liu, A. L. Ahumada, E. Bayraktar, P. Schwartz, M. Chowdhury, S. Shi, M. M. Sebastian, H. Khant, N. de Val, N. N. Bayram, G. Zhang, T. C. Vu, Z. Jie, N. B. Jennings, C. Rodriguez-Aguayo, J. Swain, E. Stur, L. S. Mangala, Y. Wu, S. Nagaraju, B. Ermias, C. Li, G. Lopez-Berestein, J. Braam and A. K. Sood, *J. Controlled Release*, 2023, **357**, 472–483.

17 R. Puupponen-Pimiä, L. Nohynek, J. Suvanto, J.-P. Salminen, T. Seppänen-Laakso, J. Tähtiharju, K. Honkapää and K.-M. Oksman-Caldentey, *ACS Food Sci. Technol.*, 2021, **1**, 917–927.

18 C. Stanly, H. Kim, G. Antonucci, I. Fiume, M. Guescini, K. P. Kim, M. A. Ciardiello, I. Giangrieco, A. Mari and G. Pocsfalvi, *Front. Bioeng. Biotechnol.*, 2021, **9**, 760730.

19 K. A. Kopf-Bolanz, F. Schwander, M. Gijs, G. Vergères, R. Portmann and L. Egger, *J. Nutr.*, 2012, **142**, 245–250.

20 J. Roerig, L. Schiller, H. Kalwa, G. Hause, C. Vissiennon, M. C. Hacker, C. Wölk and M. Schulz-Siegmund, *Eur. J. Pharm. Biopharm.*, 2021, **166**, 61–74.

21 I. Hubatsch, E. G. E. Ragnarsson and P. Artursson, *Nat. Protoc.*, 2007, **2**, 2111–2119.

22 M. Zhang, B. Xiao, H. Wang, M. K. Han, Z. Zhang, E. Viennois, C. Xu and D. Merlin, *Mol. Ther.*, 2016, **24**, 1783–1796.

23 F. Perut, L. Roncuzzi, S. Avnet, A. Massa, N. Zini, S. Sabbadini, F. Giampieri, B. Mezzetti and N. Baldini, *Biomolecules*, 2021, **11**, 87.

24 A. Mukhopadhya, J. Santoro and L. O'Driscoll, *STAR Protoc.*, 2021, **2**, 100821.

25 A. Li, D. Li, Y. Gu, R. Liu, X. Tang, Y. Zhao, F. Qi, J. Wei and J. Liu, *Acta Pharm. Sin. B*, 2023, **13**, 3300–3320.

26 J. Webber and A. Clayton, *J. Extracell. Vesicles*, 2013, **2**, 19861.

27 K. K. Jackson, C. Mata and R. K. Marcus, *Talanta*, 2023, **252**, 123779.

28 A. Steć, M. Chodkowska, J. Kasprzyk-Pochopień, P. Mielczarek, W. Piekoszewski, B. Lewczuk, A. Płoska, L. Kalinowski, B. Wielgomas and S. Dziomba, *Food Chem.*, 2023, **424**, 136333.

29 Y. Leng, L. Yang, S. Pan, L. Zhan and F. Yuan, *Food Sci. Hum. Wellness*, 2024, **13**, 869–878.

30 Y. Ito, K. Taniguchi, Y. Kuranaga, N. Eid, Y. Inomata, S.-W. Lee and K. Uchiyama, *Int. J. Mol. Sci.*, 2021, **22**, 3749.

31 J. Liu, F. Wang, Z. Weng, X. Sui, Y. Fang, X. Tang and X. Shen, *Genomics*, 2020, **112**, 2949–2958.

32 V. Lenders, X. Koutsoumpou, P. Phan, S. J. Soenen, K. Allegaert, S. de Vleeschouwer, J. Toelen, Z. Zhao and B. B. Manshian, *Chem. Soc. Rev.*, 2023, **52**, 4672–4724.

33 J. Grießinger, S. Dünnhaupt, B. Cattoz, P. Griffiths, S. Oh, S. B. i. Gómez, M. Wilcox, J. Pearson, M. Gumbleton, M. Abdulkarim, I. Pereira de Sousa and A. Bernkop-Schnürch, *Eur. J. Pharm. Biopharm.*, 2015, **96**, 464–476.

34 B. Poinard, S. Kamaluddin, A. Q. Q. Tan, K. G. Neoh and J. C. Y. Kah, *ACS Appl. Mater. Interfaces*, 2019, **11**, 4777–4789.

35 B. Tafech, M.-R. Rokhforouz, J. Leung, M. M. H. Sung, P. J. C. Lin, D. D. Sin, D. Lauster, S. Block, B. S. Quon, Y. Tam, P. Cullis, J. J. Feng and S. Hedtrich, *Adv. Healthcare Mater.*, 2024, **13**, 2304525.

36 N. Thirawong, R. A. Kennedy and P. Sriamornsak, *Carbohydr. Polym.*, 2008, **71**, 170–179.

37 A. Wilińska, A. S. de Figueiredo Rodrigues, J. Bryjak and M. Polakovič, *J. Food Eng.*, 2008, **85**, 459–465.

38 M. Vitulo, E. Gnodi, R. Meneveri and D. Barisani, *Int. J. Mol. Sci.*, 2022, **23**, 4339.

39 M. Zhang, E. Viennois, M. Prasad, Y. Zhang, L. Wang, Z. Zhang, M. K. Han, B. Xiao, C. Xu, S. Srinivasan and D. Merlin, *Biomaterials*, 2016, **101**, 321–340.

40 J. Mu, X. Zhuang, Q. Wang, H. Jiang, Z.-B. Deng, B. Wang, L. Zhang, S. Kakar, Y. Jun, D. Miller and H.-G. Zhang, *Mol. Nutr. Food Res.*, 2014, **58**, 1561–1573.

41 C. Bai, J. Liu, X. Zhang, Y. Li, Q. Qin, H. Song, C. Yuan and Z. Huang, *Biomed. Pharmacother.*, 2024, **174**, 116543.

42 Q. Chen, Q. Li, Y. Liang, M. Zu, N. Chen, B. S. B. Canup, L. Luo, C. Wang, L. Zeng and B. Xiao, *Acta Pharm. Sin. B*, 2022, **12**, 907–923.

43 K. Seo, J. H. Yoo, J. Kim, S. J. Min, D. N. Heo, I. K. Kwon and H.-J. Moon, *Nanoscale*, 2023, **15**, 5798–5808.

44 Y. Wang, M. Li, X. Xu, W. Tang, L. Xiong and Q. Sun, *J. Agric. Food Chem.*, 2019, **67**, 2296–2306.

45 X. Wang, C. Xin, Y. Zhou and T. Sun, *Pharmaceutics*, 2024, **16**, 588.

46 X. Ou, H. Wang, H. Tie, J. Liao, Y. Luo, W. Huang, R. Yu, L. Song and J. Zhu, *J. Nanobiotechnol.*, 2023, **21**, 160.

47 C. Liu, X. Yan, Y. Zhang, M. Yang, Y. Ma, Y. Zhang, Q. Xu, K. Tu and M. Zhang, *J. Nanobiotechnol.*, 2022, **20**, 206.

48 R. Ghaffarian and S. Muro, *J. Visualized Exp.*, 2013, e50638.

49 Y. He, M. Cheng, R. Yang, H. Li, Z. Lu, Y. Jin, J. Feng and L. Tu, *Nanomaterials*, 2023, **15**, 1141.

50 B. Srinivasan, A. R. Kolli, M. B. Esch, H. E. Abaci, M. L. Shuler and J. J. Hickman, *SLAS Technol.*, 2015, **20**, 107–126.

51 M. Kus, I. Ibragimow and H. Piotrowska-Kempisty, *Pharmaceutics*, 2023, **15**, 2523.

52 L. Delon, R. J. Gibson, C. A. Prestidge and B. Thierry, *J. Controlled Release*, 2022, **343**, 584–599.

53 J. Liu, X. Xie, T. Wang, H. Chen, Y. Fu, X. Cheng, J. Wu, G. Li, C. Liu, H. Liimatainen, Z. Zheng, X. Wang and D. L. Kaplan, *ACS Appl. Mater. Interfaces*, 2023, **15**, 12696–12707.

54 M. Kim and J. H. Park, *Polymers*, 2022, **14**, 1615.

55 M. K. Kim, Y. C. Choi, S. H. Cho, J. S. Choi and Y. W. Cho, *Tissue Eng. Regener. Med.*, 2021, **18**, 561–571.

56 S. Ju, J. Mu, T. Dokland, X. Zhuang, Q. Wang, H. Jiang, X. Xiang, Z.-B. Deng, B. Wang, L. Zhang, M. Roth, R. Welti, J. Mobley, Y. Jun, D. Miller and H.-G. Zhang, *Mol. Ther.*, 2013, **21**, 1345–1357.

57 E. Błeszyńska, Ł. Wierucki, T. Zdrojewski and M. Renke, *Medicina*, 2020, **56**, 320.

58 E. Lázaro-Ibáñez, F. N. Faruqu, A. F. Saleh, A. M. Silva, J. Tzu-Wen Wang, J. Rak, K. T. Al-Jamal and N. Dekker, *ACS Nano*, 2021, **15**, 3212–3227.

59 E. Reeve, S. C. Trenaman, K. Rockwood and S. N. Hilmer, *Expert Opin. Drug Metab. Toxicol.*, 2017, **13**, 651–668.

60 R. An, E. Wilms, A. A. M. Masclee, H. Smidt, E. G. Zoetendal and D. Jonkers, *Gut*, 2018, **67**, 2213.

61 X. Zhuang, Z.-B. Deng, J. Mu, L. Zhang, J. Yan, D. Miller, W. Feng, C. J. McClain and H.-G. Zhang, *J. Extracell. Vesicles*, 2015, **4**, 28713.

62 P. R. Holt, *Dig. Dis.*, 2007, **25**, 144–150.

63 M. J. Saffrey, *AGE*, 2014, **36**, 1019–1032.

64 C. Liu, D. Chu, K. Kalantar-Zadeh, J. George, H. A. Young and G. Liu, *Adv. Sci.*, 2021, **8**, 2004433.

65 I. M. Rea, D. S. Gibson, V. McGilligan, S. E. McNerlan, H. D. Alexander and O. A. Ross, *Front. Immunol.*, 2018, **9**, 586.

66 T. N.-G. Nguyen, C. V. Pham, R. Chowdhury, S. Patel, S. K. Jaysawal, Y. Hou, H. Xu, L. Jia, A. Duan, P. H.-L. Tran and W. Duan, *Pharmaceutics*, 2023, **15**, 2115.